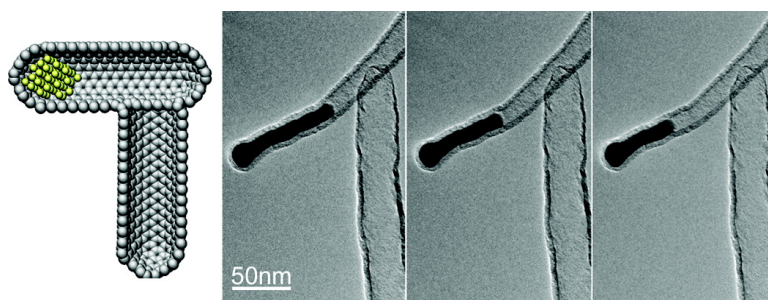


Nanotube Fluidic Junctions: Internanotube Attogram Mass Transport through Walls

Lixin Dong, Xinyong Tao, Mustapha Hamdi, Li Zhang,
Xiaobin Zhang, Antoine Ferreira, and Bradley J. Nelson

Nano Lett., **2009**, 9 (1), 210-214 • DOI: 10.1021/nl8027747 • Publication Date (Web): 12 December 2008

Downloaded from <http://pubs.acs.org> on February 11, 2009



More About This Article

Additional resources and features associated with this article are available within the HTML version:

- Supporting Information
- Access to high resolution figures
- Links to articles and content related to this article
- Copyright permission to reproduce figures and/or text from this article

[View the Full Text HTML](#)

Nanotube Fluidic Junctions: Internanotube Attogram Mass Transport through Walls

Lixin Dong,^{*,†,‡} Xinyong Tao,^{‡§} Mustapha Hamdi,^{||} Li Zhang,[†] Xiaobin Zhang,[‡]
Antoine Ferreira,^{||} and Bradley J. Nelson[†]

*Institute of Robotics and Intelligent Systems, ETH Zurich,
CH-8092 Zurich, Switzerland, Department of Materials Science and Engineering,
Zhejiang University, Hangzhou 310027, China, College of Chemical Engineering and
Materials Science, Zhejiang University of Technology, Hangzhou 310032, China, and
Institut PRISME, ENSI Bourges, 88 Boulevard Lahitolle, 18000 Bourges, France*

Received September 12, 2008; Revised Manuscript Received November 25, 2008

ABSTRACT

We report an experimental and theoretical investigation into mass transport between individual carbon nanotubes (CNTs) via their central cores. These CNT fluidic junctions can serve as basic elements for more complex nanofluidic systems and can also provide a structure for testing theories of fluid flow at the nanoscale. Controlled melting, evaporation, and flowing of copper and tin within and between nanotube shells are investigated experimentally. Cap-to-wall and wall-to-cap mass flow are realized by electric current driven heating, diffusion, and electromigration under low bias voltages between 1.5 and 1.8 V. A comparison shows that the mass loss for the cap-to-wall architecture is much smaller than that for the wall-to-cap junction. A molecular dynamics simulation is presented that provides further insight into the transport mechanism.

Growing interest in nanofluidics^{1–3} has been motivated by potential applications in mass and energy storage and transport,^{4,5} single molecule analysis,⁶ drug delivery,^{7–9} and electronics.¹⁰ The most fundamental element in a nanofluidic system is the nanochannel, which can be defined as a channel with at least one cross section smaller than 100 nm. One method of creating nanochannels is through a bottom-up approach¹¹ in which nanofluidic systems of the future could be built by assembling as-synthesized or as-fabricated building blocks such as channels, valves, pumps, mixers, separators, sensors, actuators, etc.

With their hollow cores and large aspect ratios,^{12–14} carbon nanotubes (CNTs) are prime candidates for conduits within nanofluidic systems. A variety of materials have been encapsulated by CNTs such as metals and their compounds,^{15–17} water,^{18,19} and fullerenes,²⁰ and applications of devices as templates,²¹ thermometers,²² and nano test tubes²³ have been described. The possibility of delivering²⁴ encapsulated material from the carbon shells is of great interest because of potential applications as atom-level sources for

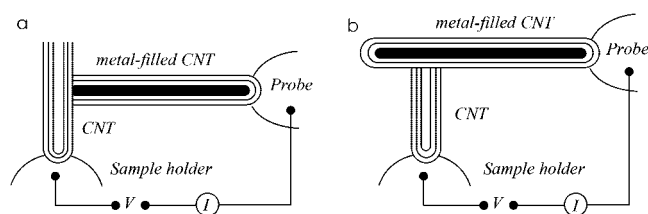


Figure 1. Schematic setup of internanotube mass transport (a) cap-to-wall transport (b) wall-to-cap transport.

nanoprototyping, nanoassembly, and injection. We previously presented an experimental investigation of controlled melting and flowing of single crystalline copper²⁵ from individual CNTs assisted by nanorobotic manipulation,²⁶ and its application in spot welding of nanotubes using this copper.⁵ A very low current induces the melting and drives the flow, which is far more efficient than irradiation-based techniques involving high energy electron beams,^{27–30} focused-ion beams (FIB),³¹ or lasers.¹⁴ Furthermore, conservation of the material is facilitated by its encapsulation as opposed to conveying mass on the external surface of nanotubes.³² Because both the rate and direction of mass transport depend on the external electrical drive, precise control and delivery of minute amounts of material is possible, and we have demonstrated controlled delivery of attograms of mass from carbon shell barriers.⁵

* To whom correspondence should be addressed. E-mail: ldong@ethz.ch.

[†] ETH Zurich.

[‡] Zhejiang University.

[§] Zhejiang University of Technology.

^{||} Institut PRISME, ENSI Bourges.

[†] Current address: Department of Electrical and Computer Engineering, Michigan State University, East Lansing, Michigan 48824-1226.

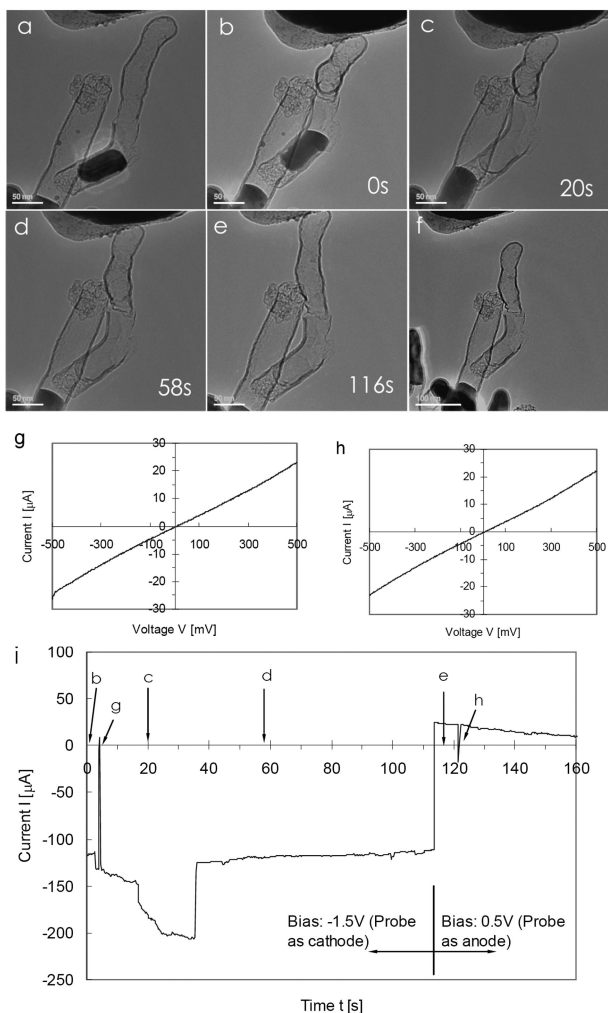


Figure 2. Cap-to-wall internanotube mass (Sn) transport. (a) A nanotube fluidic junction approaches a probe. (b–e) The process of internanotube flowing. (f) The nanotube fluidic junction is detached from the probe. Scale bars: (a–e) 50 nm, (f) 100 nm. (g,h) I – V curves recorded at $t = 4$ and 122 s. (i) Current recorded with a multimeter (sampling rate: 4 Hz). It can be seen from the time scale the moment the images b–e and the I – V curves in panels g and h were taken. The amplitudes of the peaks in panel i for the I – V curves in panels g and h are not as accurate as those shown in panels g and h due to the low sampling rate. It can be seen from the sequence that as Sn entered the junction point ($t = 20$ s), the absolute value of the current increased, showing Sn improved the contact between the two CNTs. Then a sharp drop appeared at 37.25 s, suggesting Sn left from the junction point. The current (absolute value) decreases slowly after until the bias changed polarity at 116 s. This is due to the shortening of the Sn core, which exposes the carbon shells (with larger resistance). After the polarity and value of the bias changed to 0.5 V, the current continues dropping implying a decrease of Sn on the contact between the lower CNT and the sample holder.

Previous nanofluidic investigations have been pursued using a single nanotube or an array of parallel nanotubes.^{5,12,22,24,33–35} To construct more complex fluidic systems, interconnection of individual nanochannels is needed, where nanofluidic junctions as shown in Figure 1 serve as fundamental fluidic elements. Here we present nanotube fluidic junctions for internanotube mass transport using the architectures illustrated in Figure 1.

The samples we use include Cu-tipped and Sn-filled CNTs. As described elsewhere, the Cu-tipped CNT samples are synthesized using an alkali-doped Cu catalyst by a thermal chemical vapor deposition (CVD) method.²⁵ The CNTs are up to 5 μm long with outer diameters in a range of 40–80 nm. The single crystalline Cu nanoneedles are encapsulated in graphite walls approximately 4 to 6 nm thick at the tips of CNTs. Sn-filled CNTs are synthesized by catalytic deposition of acetylene using nanocrystalline SnO_2 as a catalyst. A one-step CVD method was adopted for the synthesis of Sn-filled CNTs, that is, the catalyst was directly introduced into the hot furnace without a preheating and reduction process. The CNTs have a diameter distribution from 20 to 80 nm. Sn cores are single crystal with good crystallization, while the CNTs consist of disordered carbon sheets with small areas of roughly aligned graphite.

Our experiments were performed in a transmission electron microscope (TEM, Philips CM30) equipped with a scanning tunneling microscope (STM) built in a TEM holder (Nanofactory Instruments AB, ST-1000) serving as a manipulator. The material consisting of a CNT bundle is attached to a 0.35 mm thick Au wire using silver paint, and the wire is held in the specimen holder (Figure 1). Two kinds of probes are used. One type is an etched 10 μm thick tungsten wire with a tip radius of approximately 100 nm (Picoprobe, T-4-10-1 mm), and the other type is an atomic force microscope (AFM) cantilever (Mikromasch, CSC38/Ti-Pt). The probe can be positioned in a millimeter-scale workspace with subnanometer resolution with the STM unit actuated by a three-degree-of-freedom piezo-tube, making it possible to select a specific CNT and pick it up. Physical contact can be made between the probe and the tip of a nanotube or between two nanotubes. Applying a voltage between the probe and the sample holder establishes an electrical circuit through a CNT or a CNT junction and injects thermal energy into the system via Joule heating. By increasing the applied voltage, the local temperature can be increased past the melting point of the material encapsulated in a tube. The process is recorded by TEM images, a multimeter, and a nA meter.

Figure 2 shows cap-to-wall internanotube mass (Sn) transport. Figure 2a is a TEM image of a nanotube fluidic junction, which includes two Sn-filled CNTs. The upper CNT has its opened cap attached on the walls of the lower tube. The junction is then attached to a probe. Parts b–e of Figure 2 show the process of internanotube mass flow. Figure 2f shows that the nanotube fluidic junction is detached from the probe. Figure 2g,h are I – V curves recorded at $t = 4$ and 122 s, respectively. It can be seen that no obvious changes occurred before and after flowing, suggesting that there is no significant altering of the carbon shells. Figure 2i is the current recorded with a multimeter (sampling rate: 4 Hz). It can be seen from the time scale the moments when the images (parts b–e of Figure 2) and the I – V curves (parts g and h of Figure 2) were taken. The amplitudes of the peaks in Figure 2i for g and h are not as accurate as that shown in parts g and h of Figure 2 due to the low sampling rate. It can be seen from the sequence that as Sn entered the junction

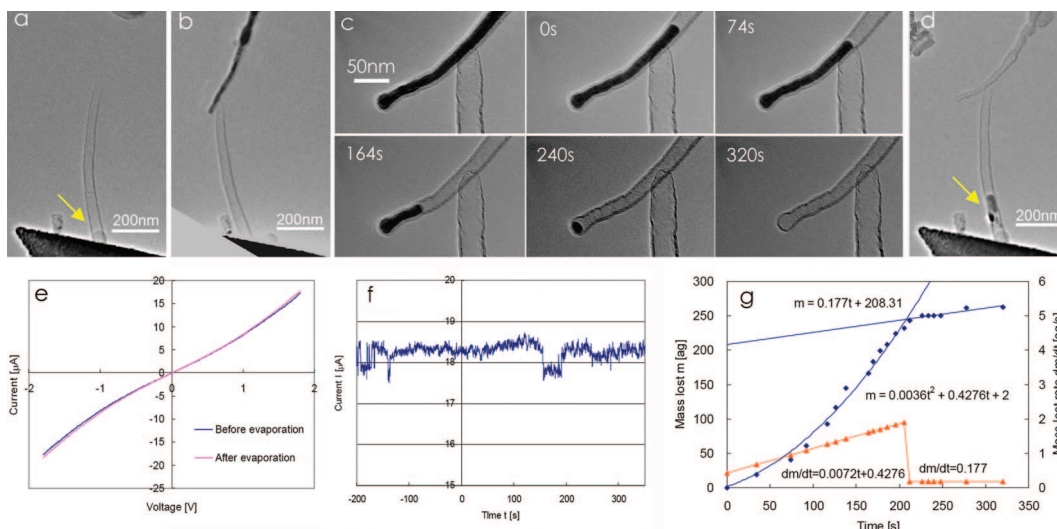


Figure 3. Wall-to-cap internanotube mass (Cu) transport. (a) Before attaching to the Cu-CNT. (b) Attaching to the Cu-CNT. (c) Attached to the Cu-CNT and the process of internanotube flowing. (d) After evaporation. (e) I - V curves before and after evaporation (probe as cathode). (f) Current vs time monitored with a multimeter (sampling rate: 4 Hz) shows there was no obvious change when the copper was transported ($t = 0$ – 320 s). (g) Mass lost from the Cu-tipped CNT and the mass flow rate.

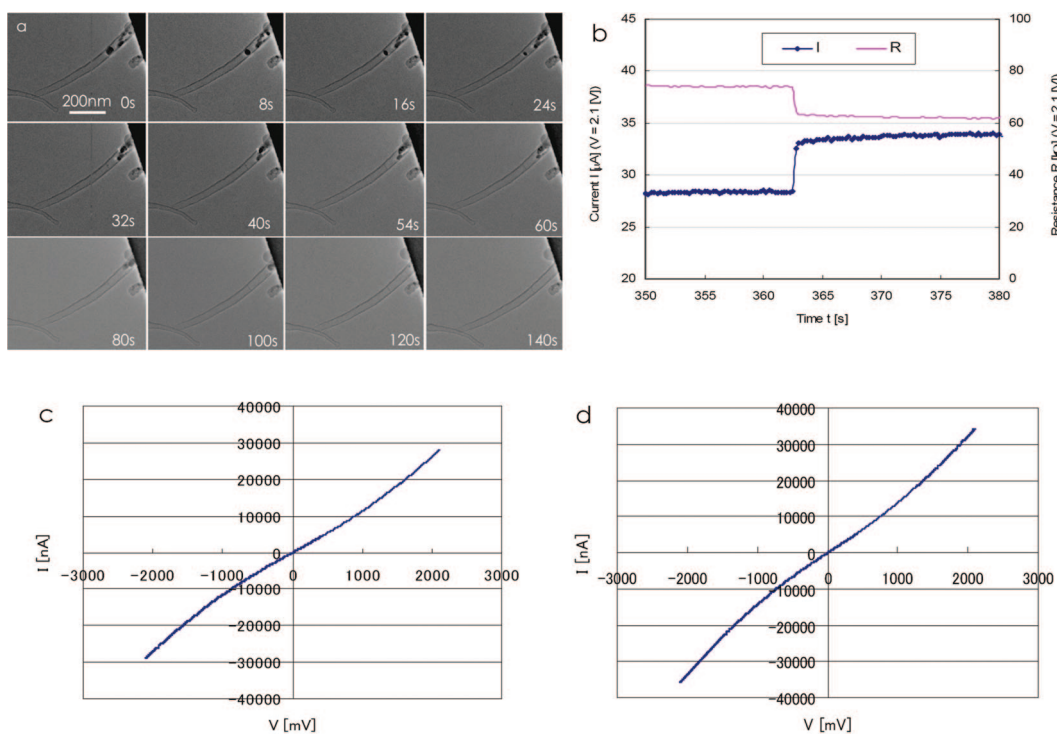


Figure 4. Intrananotube mass (Cu) transport. (a) Flow of copper (bias 2.1 V) from the cap-opened CNT to the electrode (a Pt-coated AFM cantilever). (b) Contact resistance improved when copper diffused onto the AFM cantilever (cantilever as anode). (c,d) I - V curves show the contact resistance improved when copper diffused onto the cantilever: (c) before melting and (d) after melting.

point ($t = 20$ s), the absolute value of the current increased, indicating Sn improved the contact between the two CNTs. Then a sharp drop appeared at 37.25 s, suggesting Sn left from the junction point. The current (absolute value) decreased slowly afterward until the bias changed polarity at 116 s. This is due to the shortening of the Sn core, which exposes the carbon shells (and increases the resistance). After the polarity and value of the bias changed to 0.5 V, the current continues dropping implying a decrease of Sn on the contact between the lower CNT and the sample holder.

According to the geometry and the density of Sn (7.31 g/cm^3), the original mass is approximately 662 ag (Figure 2b), whereas the received mass by the lower tube is 377 ag (Figure 2c), that is, 56.9% of the original mass is transported from the upper tube to the lower one.

Figure 3 presents wall-to-cap internanotube mass (Cu) transport. Figure 3a shows a tube before attachment to a Cu-tipped CNT, whereas Figure 3b shows a junction is formed when a Cu-tipped CNT attached to the tube. Figure 3c is the process of internanotube flowing (a video compiled from

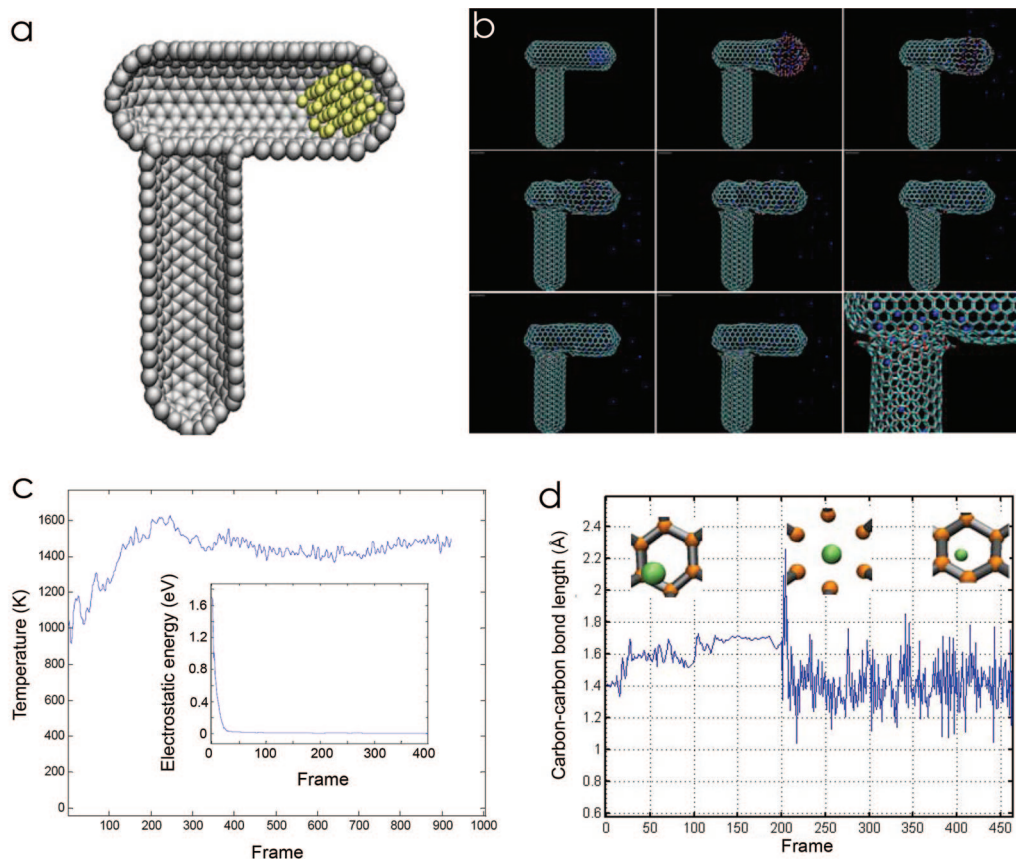


Figure 5. Molecular dynamics simulation of intertube mass (Cu) transport. (a) Initial configuration of the simulated system with a cut view. Copper cluster is yellow. (b) Frames of melting and intertube diffusion of the Cu cluster using molecular dynamics simulation. (c) Melting temperature of copper crystal during simulation. The inset shows the electrostatic repulsive energy between copper ions during melting. (d) Carbon-carbon bond length during copper diffusion. At frame 200 the copper ions pass through the hexagonal rings, which correspond to the maximum opening of the carbon rings.

more images is available online as Supporting Information), and Figure 3d shows after evaporation. Figure 3e shows $I-V$ curves before and after evaporation (probe as cathode). Figure 3f depicts current versus time monitored with a multimeter (sampling rate: 4 Hz) demonstrating no obvious change when the copper was transported ($t = 0-320$ s). Figure 3g shows the mass lost from the Cu-tipped CNT and the mass flow rate as determined by line fitting. According to the apparent volume and the density of Cu (8.92 g/cm^3), the original mass is approximately 2804 ag (Figure 3b), whereas the received mass by the lower tube is 746 ag (Figure 3d), that is, 26.6% of the original mass is transported from the upper tube to the lower one, which is less than half of the transport for the cap-to-wall configuration. Nevertheless, considering that the opened area of the lower tube is only a very small portion (6%) of the entire surface area of the upper tube that allows Cu atoms to escape, the effect of the electric field is obvious.

Figure 4 shows intranotube mass (Cu) transport as the continuation of Figure 3d. Figure 4a reveals flowing of the received copper (as indicated with the arrows, bias 2.1 V) from the cap-opened CNT onto the electrode (a Pt-coated AFM cantilever). It can be seen from Figure 4b that the contact resistance improved when copper diffused onto the AFM cantilever which served as the anode. Parts c and d of Figure 4 are $I-V$ curves shown the contact resistance

improved when copper diffused onto the cantilever before melting (Figure 4c) and after melting (Figure 4d).

As having been discussed in the previous investigation on current-driven intranotube flow, the most probable mechanism for the observed flow in the fluidic junctions is electromigration.^{5,24} Other possible mechanisms such as capillary forces, thermal expansion, and shell-shrinkage-induced flow can be excluded. To understand how the mass passed through the walls, we numerically investigated intertube mass (Cu) transport using molecular dynamics simulation (MDS) (Figure 5). Figure 5a shows the initial atomic configuration of the simulated wall-to-cap transport system. The potential energy of the wall-to-cap transport system with a cluster of Cu inside was minimized at an internal pressure of 1 atm using the conjugate gradient method. To investigate copper diffusion, the system was simulated at temperatures between 700 and 1800 K using molecular dynamics. The position of the copper ions as shown in the frames in Figure 5b indicate that the copper has melted and diffused. The system temperature during diffusion is shown by the curve in Figure 5c. An analysis of the repulsive electrostatic energy between copper ions is given in the inset of Figure 5c. It can be seen that a peak temperature was reached at frame 200. Accordingly, as shown in Figure 5d, the carbon-carbon bond length obtained a maximum value at frame 200. The simulation indicates

that electric energy is responsible for heating, and that the repulsive charges increase the distances between copper ions and induce their transport. It can be seen from Figure 5d that with a large enough charge, copper ions can pass through the walls of CNTs without necessarily breaking the bonds. Images clearly show that the hexagon carbon rings stretch during diffusion. Simulation also revealed that electrostatic forces guide the motion of the copper ions, causing the ions to collect in the original empty tube. It can be deduced that by increasing the number of shells, mass lost through the walls can be decreased. To realize internanotube transport, thinner shells are critical for keeping the mobility of the ions. Hence, an optimization of the number of shells will be needed when designing a fluidic system for a specific application.

In summary, controlled melting, evaporation and flowing of copper and tin internanotube shells have been investigated experimentally. Cap-to-wall and wall-to-cap mass flow are realized by electric current driven heating, diffusion, and electromigration under low bias voltages between 1.5 and 1.8 V. A comparison shows that the mass loss for the cap-to-wall architecture is much smaller than that for the wall-to-cap junction. It should be noted that cap-to-wall and wall-to-cap mass flow can occur in the same fluidic junction for a reversible transport. For example, if the direct flow is cap-to-wall, the reverse flow will be wall-to-cap, and vice versa. This structure-related reversibility in fluidic junctions is different from that in an individual channel.^{5,24} Dynamic simulation of intertube copper transport indicates that charge increases the distance between copper ions and then induces the transport of copper ions. Copper ions pass through the walls of CNTs without necessarily breaking the bonds, and the hexagonal carbon rings stretch during diffusion.

Acknowledgment. This work is conducted with financial support from the ETH Zurich and the Chinese National Science Foundation (No. 50571087), the Hi-tech Research and Development Program of China (863) (2002 AA334020), and the Natural Sciences Fund of Zhejiang Province (Y404274). The authors would like to thank the support of the Electron Microscopy Center of ETH Zurich (EMEZ).

Supporting Information Available: A video (AVI) compiled from more images than shown in Figure 3c shows the dynamic process. This material is available free of charge via the Internet at <http://pubs.acs.org>.

References

(1) Eijkel, J. C. T.; van den Berg, A. *Microfluid. Nanofluid.* **2005**, *1* (3), 249–267.

(2) Goldberger, J.; Fan, R.; Yang, P. D. *Acc. Chem. Res.* **2006**, *39* (4), 239–248.

(3) Mattia, D.; Gogotsi, Y. *Microfluid. Nanofluid.* **2008**, *5* (3), 289–305.

(4) van der Heyden, F. H. J.; Bonthuis, D. J.; Stein, D.; Meyer, C.; Dekker, C. *Nano Lett.* **2006**, *6* (10), 2232–2237.

(5) Dong, L. X.; Tao, X. Y.; Zhang, L.; Zhang, X. B.; Nelson, B. J. *Nano Lett.* **2007**, *7* (1), 58–63.

(6) Dekker, C. *Nat. Nanotechnol.* **2007**, *2* (4), 209–215.

(7) Freedman, J. R.; Mattia, D.; Korneva, G.; Gogotsi, Y.; Friedman, G.; Fontecchio, A. K. *Appl. Phys. Lett.* **2007**, *90* (10), 103108.

(8) Chen, X.; Kis, A.; Zettl, A.; Bertozzi, C. R. *Proc. Natl. Acad. Sci. U.S.A.* **2007**, *104* (20), 8218–8222.

(9) Schrlau, M. G.; Falls, E. M.; Ziober, B. L.; Bau, H. H. *Nanotechnology* **2008**, *19* (1), 4–015101.

(10) Daiguji, H.; Oka, Y.; Shirono, K. *Nano Lett.* **2005**, *5* (11), 2274–2280.

(11) Mijatovic, D.; Eijkel, J. C. T.; van den Berg, A. *Lab Chip* **2005**, *5* (5), 492–500.

(12) Whitby, M.; Quirke, N. *Nat. Nanotechnol.* **2007**, *2* (2), 87–94.

(13) Supple, S.; Quirke, N. *Phys. Rev. Lett.* **2003**, *90* (21), 214501.

(14) Kral, P.; Tomanek, D. *Phys. Rev. Lett.* **1999**, *82* (26), 5373–5376.

(15) Ajayan, P. M.; Iijima, S. *Nature* **1993**, *361* (6410), 333–334.

(16) Tsang, S. C.; Chen, Y. K.; Harris, P. J. F.; Green, M. L. H. *Nature* **1994**, *372* (6502), 159–162.

(17) Ajayan, P. M.; Colliex, C.; Lambert, J. M.; Bernier, P.; Barbedette, L.; Tence, M.; Stephan, O. *Phys. Rev. Lett.* **1994**, *72* (11), 1722–1725.

(18) Gogotsi, Y.; Libera, J. A.; Guvenc-Yazicioglu, A.; Megaridis, C. M. *Appl. Phys. Lett.* **2001**, *79* (7), 1021–1023.

(19) Holt, J. K. *Microfluid. Nanofluid.* **2008**, *5* (4), 425–442.

(20) Smith, B. W.; Monthieux, M.; Luzzi, D. E. *Nature* **1998**, *396* (6709), 323–324.

(21) Ajayan, P. M.; Stephan, O.; Redlich, P.; Colliex, C. *Nature* **1995**, *375* (6532), 564–567.

(22) Gao, Y. H.; Bando, Y. *Nature* **2002**, *415* (6872), 599–599.

(23) Ugarte, D.; Chatelain, A.; de Heer, W. A. *Science* **1996**, *274* (5294), 1897–1899.

(24) Svensson, K.; Olin, H.; Olsson, E. *Phys. Rev. Lett.* **2004**, *93* (14), 145901.

(25) Tao, X. Y.; Zhang, X. B.; Cheng, J. P.; Luo, Z. Q.; Zhou, S. M.; Liu, F. *Diamond Relat. Mater.* **2006**, *15* (9), 1271–1275.

(26) Dong, L. X.; Arai, F.; Fukuda, T. *IEEE-ASME Trans. Mechatronics* **2004**, *9* (2), 350–357.

(27) Dong, L. X.; Arai, F.; Fukuda, T. *Appl. Phys. Lett.* **2002**, *81* (10), 1919–1921.

(28) Madsen, D. N.; Molhave, K.; Mateiu, R.; Rasmussen, A. M.; Brorson, M.; Jacobsen, C. J. H.; Boggild, P. *Nano Lett.* **2003**, *3* (1), 47–49.

(29) Yokota, T.; Murayama, M.; Howe, J. M. *Phys. Rev. Lett.* **2003**, *91* (26), 4–265504.

(30) Xu, S. Y.; Tian, M. L.; Wang, J. G.; Xu, H.; Redwing, J. M.; Chan, M. H. W. *Small* **2005**, *1* (12), 1221–1229.

(31) Matsui, S.; Kaito, T.; Fujita, J.; Komuro, M.; Kanda, K.; Haruyama, Y. *J. Vac. Sci. Technol., B* **2000**, *18* (6), 3181–3184.

(32) Regan, B. C.; Aloni, S.; Ritchie, R. O.; Dahmen, U.; Zettl, A. *Nature* **2004**, *428* (6986), 924–927.

(33) Majumder, M.; Chopra, N.; Andrews, R.; Hinds, B. J. *Nature* **2005**, *438* (7064), 44–44.

(34) Golberg, D.; Costa, P.; Mitome, M.; Hampel, S.; Haase, D.; Mueller, C.; Leonhardt, A.; Bando, Y. *Adv. Mater.* **2007**, *19* (15), 1937–1942.

(35) Costa, P. M. F. J.; Golberg, D.; Mitome, M.; Hampel, S.; Leonhardt, A.; Buchner, B.; Bando, Y. *Nano Lett.* **2008**, *8* (10), 3120–3125.

NL8027747